of rotation (5.2) conjugate to τ_4). Show that the Hamiltonian function (5.1) turns into

$$H_\mu(q,p) \;=\; \frac{p^2}{2} - \frac{\gamma}{q} + \frac{\mu^2}{2q^2} \tag{5.9}$$

on $]0,\infty[\,\times\mathbb{R}$. △

The phase portraits of the one-degree-of-freedom problem on $\mathcal{P}_\mu$ with Hamiltonian function $H_\mu(\tau_1,\tau_2,\tau_3) = H(\tau_1,\tau_2,\tau_3,\mu)$ defined by (5.8) are given by the intersections of the energy level sets $\{H_\mu = h\} \subseteq \mathbb{R}^3$ with the phase space $\mathcal{P}_\mu \subseteq \mathbb{R}^3$. The latter is a surface of revolution (around the axis $\tau_1 = \tau_2$) and the former is a 'cylinder', a direct product $B_h \times \mathbb{R}$ on the basis

$$B_h \;=\; \left\{ (\tau_1,\tau_2)\in\mathbb{R}^2 \;\middle|\; \tau_2 = h - U(2\tau_1) \right\}$$

in $\mathbb{R}^2$. Thus, we can obtain the orbits from the relative position of the two curves $\mathcal{P}_\mu \cap \{\tau_3 = 0\}$ and $\{H_\mu(\tau_1,\tau_2,0) = h\} = B_h$ within $\mathbb{R}^2$. For $\mu = 0$ the former is the positive τ_1–axis $\{\tau_1 > 0, \tau_2 = 0\}$ and for $\mu \neq 0$ it is the hyperbola

$$\tau_2 \;=\; \frac{\mu^2}{4\tau_1}\;. \tag{5.10}$$

Fixing μ and varying the energy value h results in "moving the basis B_h up or down" and yields the phase portraits. We keep considering general potentials $U = U(2\pi_1)$, but for explicit computations (and the resulting formulas below) we specialize to the Newtonian potential U derived from (5.1b) where we obtain Fig. 5.1. This then easily yields the phase portraits in Fig. 5.2.

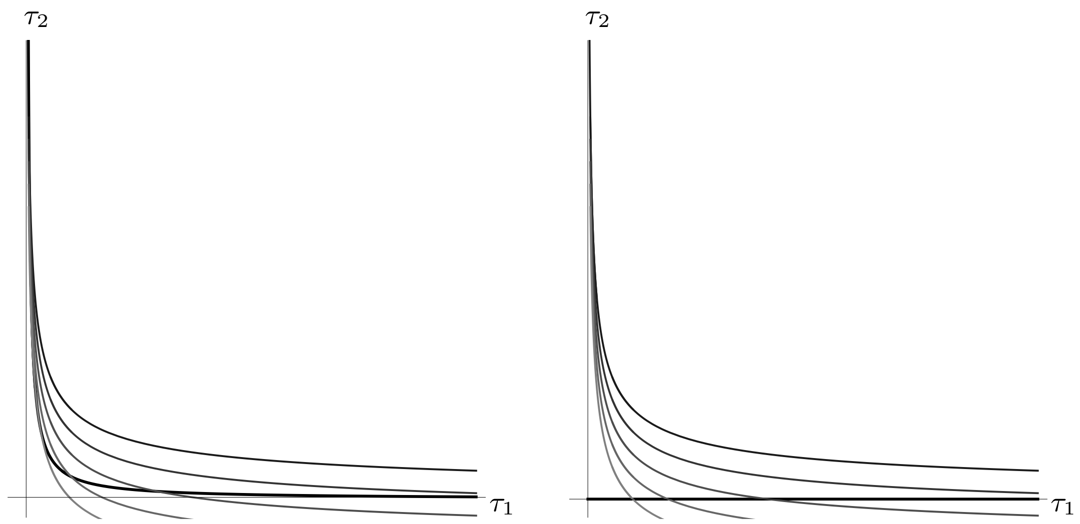

Fig. 5.1. Intersection within the (τ_1,τ_2)–plane of the reduced phase space $\mathcal{P}_\mu$ with the level sets of the energy. **a)** for $\mu \neq 0$. **b)** for $\mu = 0$.

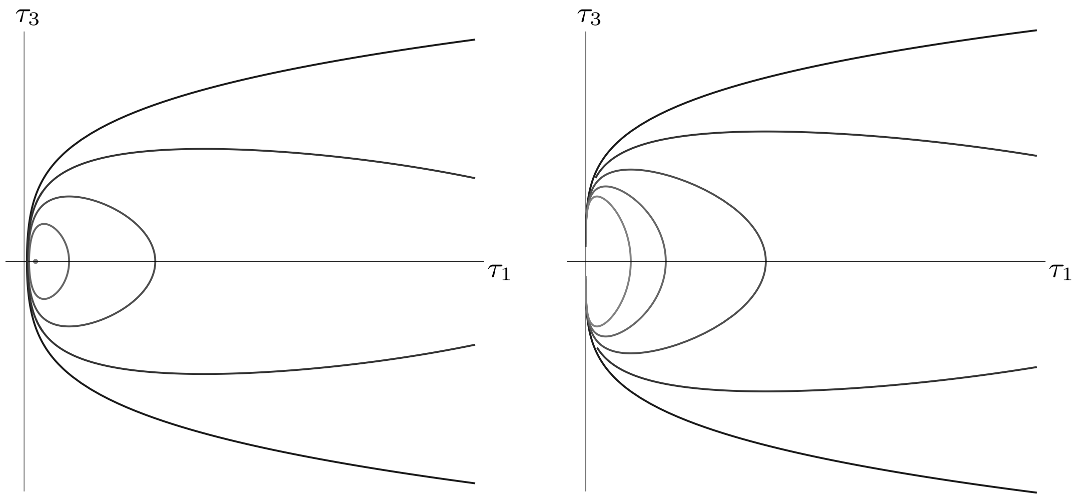

Fig. 5.2. Projection to the (τ_1, τ_3)–plane of the phase portraits obtained from Fig. 5.1. **a)** for $\mu \neq 0$. **b)** for $\mu = 0$.

The reduced flows are organized by the (relative) equilibria, where the two surfaces touch each other. This can only happen in the (τ_1, τ_2)–plane as the surface of revolution $\mathcal{P}_\mu$ has nowhere else tangent planes that contain the τ_3–axis. Equilibria are therefore given by the points where the two planar curves $\mathcal{P}_\mu \cap \{\tau_3 = 0\}$ and B_h touch. For $\mu = 0$ the strictly monotonous functions

$$\tau_2 \;=\; h + \frac{\gamma}{\sqrt{2\tau_1}} \tag{5.11}$$

obtained from (5.1b) can intersect the τ_1–axis only transversely, whence there are no equilibria in this case. For $\mu \neq 0$ the hyperbola (5.10) touches B_h if and only if the difference function

$$V_\mu(\tau_1) \;=\; U(2\tau_1) + \frac{\mu^2}{4\tau_1} - h \tag{5.12}$$

has a double zero. The equation $V_\mu(\tau_1) = 0$ can always be fulfilled by adjusting the value h of the energy accordingly. The remaining equation

$$V'_\mu(\tau_1) \;=\; 2\,U'(2\tau_1) - \frac{\mu^2}{4\tau_1^2} \;\stackrel{!}{=}\; 0$$

is for each μ an equation in τ_1 with for (5.1b) the solution

$$\tau_1 \;=\; \frac{\mu^4}{2\gamma^2} \tag{5.13a}$$

whence

$$h \;=\; \frac{-\gamma^2}{2\mu^2} \quad \text{and} \quad \tau_2 \;=\; \frac{\gamma^2}{2\mu^2} \; . \tag{5.13b}$$

In particular, the equation

$$\left(\frac{2\pi\mu^3}{\gamma^2}\right)^2 = \frac{4\pi^2}{\gamma}\left(\frac{\mu^2}{\gamma}\right)^3$$

relates period and radius as predicted by Kepler's third law.

Exercise 5.11. Derive the $\frac{1}{d}$–form of the gravitational potential, d the distance, from Kepler's third law. $\triangle$

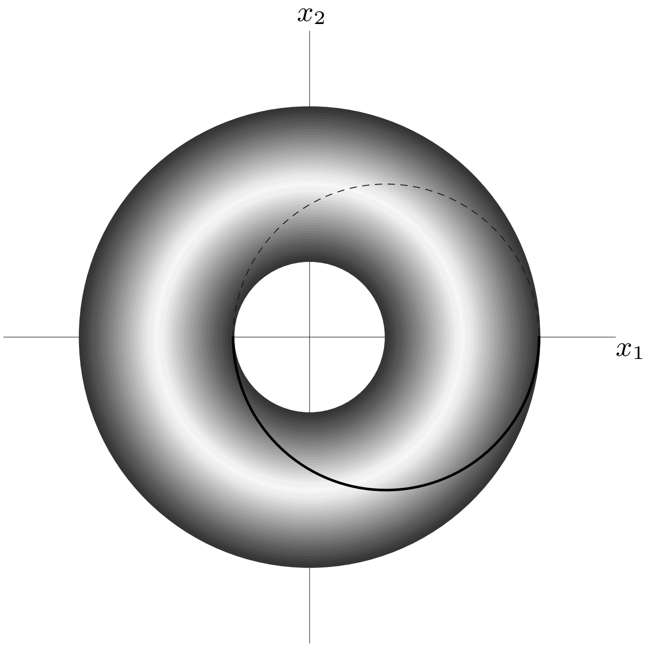

Fig. 5.3. The torus (5.14) within (x_1, x_2, τ_3)–space $\mathbb{R}^3$ seen along the τ_3–axis. A (conditionally) periodic orbit that stays within a tilted plane projects to an ellipse on the (x_1, x_2)–plane.

For periodic orbits on $\mathcal{P}_\mu$ the two intersection points of the hyperbola (5.10) and the graph of (5.11) yield an inner and an outer radius in configuration space $\mathbb{R}^2 \backslash \{0\}$ between which (the projection of) the reconstructed trajectory is captured. Passing on phase space to co-ordinates $(x_1, x_2, \tau_3, \tau_4)$, with inverse given by

$$\begin{aligned} y_1 &= \frac{x_1\tau_3 - x_2\tau_4}{x_1^2 + x_2^2} \\ y_2 &= \frac{x_2\tau_3 + x_1\tau_4}{x_1^2 + x_2^2} \end{aligned}$$

allows us to fix the fourth co-ordinate τ_4 and identify the torus

$$\left\{ (x_1, x_2, \tau_3, \tau_4) \in \mathbb{R}^4 \;\middle|\; \tau_4 = \mu \,,\, H = h \right\} \tag{5.14}$$

in Fig. 5.3. The motion on this invariant manifold is conditionally periodic, superposing the periodic motion on $\mathcal{P}_\mu$ with the periodic motion in ρ along the attached circles. In the[3] limit $h \to \frac{-\gamma^2}{2\mu^2}$ the torus shrinks down to the periodic orbit in the x–plane $\{\tau_3 = 0\}$. As h passes to positive values, the outer radius goes to infinity (and beyond) whence the torus turns into a cylinder. The flow on (5.14) commutes with the S^1–action (5.2) which turns trajectories into trajectories, only rotating x and leaving the co-ordinates τ_3 and τ_4 fixed.

Exercise 5.12. Describe the behaviour of an orbit in a (planar) central force field that has total energy equal to the effective potential energy at a local maximum. △

Exercise 5.13. What do the results on planar central force fields imply for the free particle? △

5.2 The eccentricity vector

The energy-momentum mapping

$$\begin{array}{rccc} \mathcal{EM} \; : & \mathbb{R}^4 & \longrightarrow & \mathbb{R}^2 \\ & (x, y) & \mapsto & (\tau_4(x, y), H(x, y)) \end{array} \tag{5.15}$$

allows to collect the information on the global dynamics that we obtained so far, see Fig. 5.4 for the potential (5.1b) of the Kepler system. Shown are the bifurcation values of $\mathcal{EM}$, the remaining open parts consist[4] of regular values.

For values $(\mu, h) \in \mathbb{R}^2$ satisfying $h < \frac{-\gamma^2}{2\mu^2}$ the inverse image $\mathcal{EM}^{-1}(\mu, h)$ is empty. It is only by convention that these are called regular values; with this definition the statement of Sard's Lemma is simply that the regular values of a smooth mapping form an open and dense set of full measure — the complement (the critical values) has Lebesgue measure zero. The regular values in

$$\left\{ (\mu, h) \in \mathbb{R}^2 \;\middle|\; \mu \neq 0 \,,\, \frac{-\gamma^2}{2\mu^2} < h < 0 \right\}$$

have invariant tori as inverse images, on which the periodic orbit $\mathcal{P}_\mu \cap H_\mu^{-1}(h)$ is superposed with the periodic motion in the ρ–variable that has been suppressed when reducing the symmetry (5.2).

[3] For (5.1); in general: as h approaches a minimum.

[4] Not of *the* regular values: the values on the μ– and h–axes are also regular, but the inverse image $\mathcal{EM}^{-1}(\mu, h)$ changes as the value (μ, h) crosses an axis, as it does when crossing the set $\{(\mu, h) \in \mathbb{R}^2 \mid 2\mu^2 h + \gamma = 0\}$ of singular values.

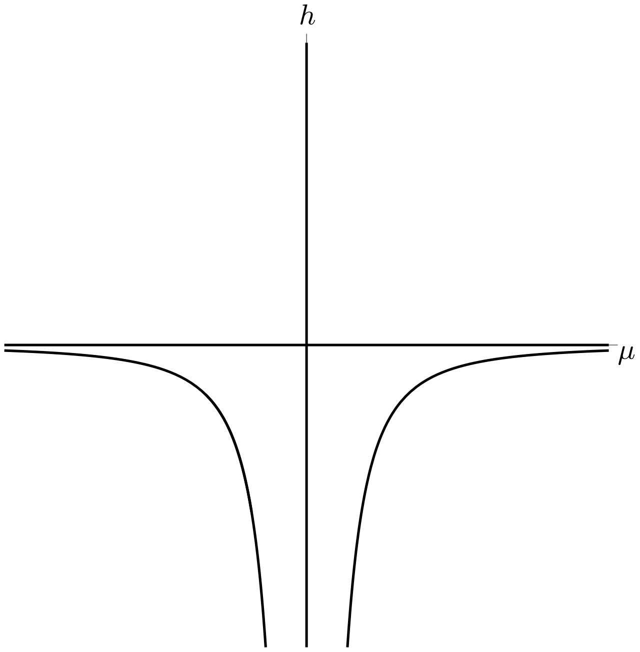

Fig. 5.4. Bifurcation values of the energy-momentum mapping of the Kepler system. The points on the hyperbolas are also critical values of $\mathcal{EM}$, while the axes consist of regular values.

For a general central force field this conditionally periodic motion alternates between quasi-periodic — the trajectory lies dense on the torus — and periodic — the trajectory returns exactly to its initial state after having superposed the two periodic motions for a finite number of periods. Furthermore, it will in general depend on the initial condition, and thus on the values μ of τ_4 and h of H, which of these two alternatives applies. A torus $\mathcal{EM}^{-1}(\mu, h)$ that consists of periodic orbits is also called resonant, since the frequencies ω_1, ω_2 satisfy a resonance relation

$$k_1\omega_1 \ + \ k_2\omega_2 \ = \ 0 \tag{5.16}$$

with an integer vector $k \in \mathbb{Z}^{2\backslash\{0\}}$ that one may choose to have relative prime components. The periodic motion then consists of k_2 periods on the reduced phase space superposed with k_1 full rotations about the origin $x = 0$.

According to Kepler's first law, all invariant 2–tori have to be resonant, with $k_1 = k_2 = 1$ in (5.16). While following an ellipse in configuration space $\mathbb{R}^{2\backslash\{0\}}$, the trajectory moves along the "lower" part of the torus when approching the origin and along the "upper" part when elongating (indeed, $\dot{\tau}_1 = \tau_3$), see Fig. 5.3. Such a uniform resonance, valid for all invariant tori simultaneously, hints to the existence of an additional conserved quantity (and hence to an extra symmetry).

Theorem 5.2. (Noether). Let $(\psi_s)_{s\in\mathbb{R}}$ be the flow of a Hamiltonian vector field defined by $F \in C^\infty(\mathcal{P})$ for which every $\psi_s : \mathcal{P} \longrightarrow \mathcal{P}$ is a symmetry of the

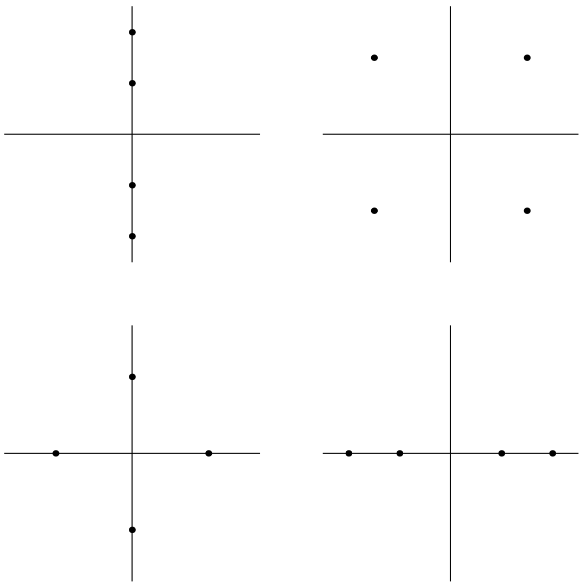

Fig. 7.1. Eigenvalue configurations of structurally stable equilibria in Hamiltonian systems with two degrees of freedom.

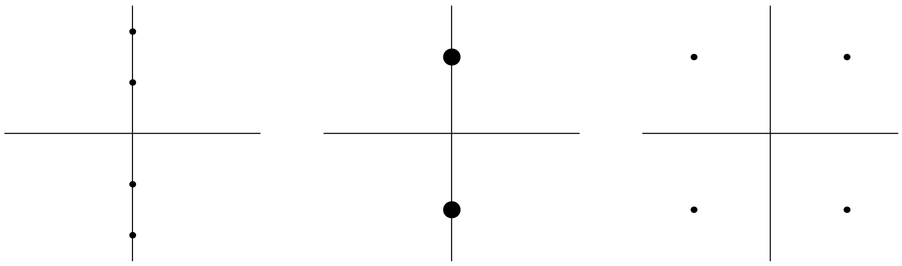

Fig. 7.2. Eigenvalue configurations undergoing a Krein collision.

Hamiltonian has a quadratic part of the form (7.1), showing that all small deformations of a 1:1 resonant equilibrium are elliptic.

Thus, a 1–parameter family H^λ of Hamiltonians with an equilibrium $z_\lambda \in \mathbb{R}^4$ passing from focus-focus type to centre-centre type has to admit a parameter value λ_0 for which the equilibrium is in 1:−1 resonance.

Exercise 7.5. Use the implicit mapping theorem to change to new co-ordinates in which $z_\lambda = 0$ for all parameter values $\lambda \in \mathbb{R}$. △

For a better understanding of the situation it is helpful to apply the co-ordinate transformation

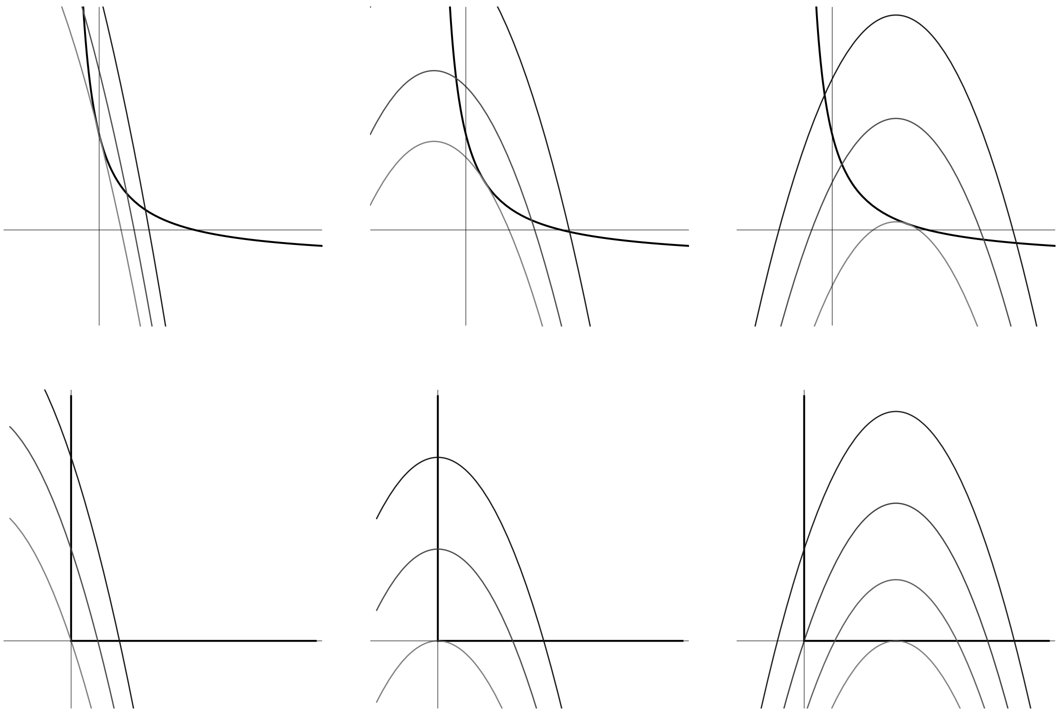

Fig. 7.3. Intersection within the (τ_2, τ_1)–plane of the reduced phase space $\mathcal{P}_\mu$ with the level sets of the energy. **a-c)** for $\mu \neq 0$. **d-f)** for $\mu = 0$. Note that in all figures the horizontal axis is the τ_2–axis and the vertical axis is the τ_1–axis.

The discriminant locus of a general polynomial of degree 3 is a cylinder on the basis of the bifurcation diagram derived in exercise 2.8, two smooth surfaces meet at one cusp line. We are interested in the way this set gets folded under the mapping

$$(\lambda, \mu, h) \quad \mapsto \quad \left(2\lambda, \frac{\mu^2}{2}, 2h \right)$$

that assigns to our parameters the coefficients of (7.13).

Lemma 7.2. The discriminant locus of (7.13) *coincides with the discriminant locus of the polynomial*

$$\tau_2^4 \; - \; \lambda \tau_2^2 \; + \; \sqrt{2}\mu\tau_2 \; + \; \frac{h}{2} \; + \; \frac{\lambda^2}{4} \; . \tag{7.14}$$

To prove this lemma just compute the two discriminant loci. The more interesting question is how to get the idea to compare these two sets. This is much easier to answer after solving exercise 7.17. The bifurcation diagram of (7.12) is the swallow tail surface which lies at the basis of the discriminant locus of the general polynomial of degree 4 (the leading 4th order term can be scaled to 1 and a translation removes the 3rd order term). With this picture in mind, we now determine the set of critical values of $\mathcal{EM}$.

Exercise 7.20. Use the translation $\tau_2 \mapsto \tau_2 - \frac{2}{3}\lambda$ to turn (7.13) into standard form $\tau_2^3 + \kappa_1\tau_2 + \kappa_2$ and study the mapping $\kappa = \kappa(\lambda, \mu, h)$ from $\mathbb{R}^3$ to $\mathbb{R}^2$. △

The mapping

$$(\lambda, \mu, h) \quad \mapsto \quad \left(\frac{\lambda}{12}, \frac{\sqrt{2}\mu}{24}, \frac{2h + \lambda^2}{96} \right)$$

that assigns to our parameters the coefficients of the partial derivative of (7.12) with respect to x, thus relating $\frac{1}{24}x^4 - \frac{1}{2}\nu_1 x^2 + \nu_2 x + \nu_3$ to (7.14), is a diffeomorphism whence the discriminant locus of (7.13) is indeed the swallow tail surface. To obtain the set of critical values of the energy-momentum mapping we still have to take the inequalities $\tau_1 \geq 0$ and $\tau_2 \geq 0$ into account. The latter is no restriction since the polynomial (7.14) is invariant under the simultaneous transformation $\tau_2 \mapsto -\tau_2$, $\mu \mapsto -\mu$ and the discriminant locus of (7.14) is symmetric with respect to the reflection in μ. The former inequality yields $h - \frac{1}{2}\tau_2^2 - \lambda\tau_2 \geq 0$ which results in $h \geq 0$ for $\lambda \geq 0$ and in $h \geq -\frac{1}{2}\lambda^2$ for $\lambda \leq 0$. Thus, we have to "remove the tail" from the swallow tail, see Fig. 7.4.a.

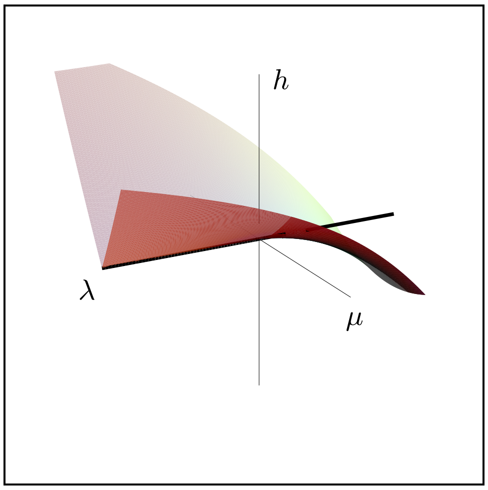

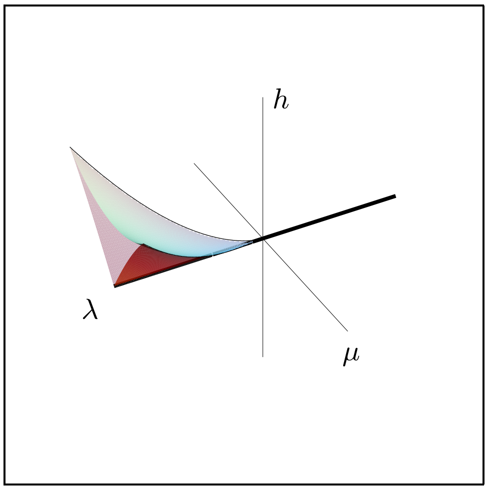

Fig. 7.4. Sketch of the set of singular values of the energy–momentum mapping $(\tau_4, \bar{H}^\lambda)$ for **a)** the supercritical case and **b)** the subcritical case.

Note that the λ–axis consists of critical values of $\mathcal{EM}$ since τ_4 and $\bar{H}^\lambda$ vanish for all λ at the origin. For $\lambda > 0$ the critical values form a crease at this line, corresponding to two families of periodic orbits that shrink down to the (stable) equilibrium. For $\lambda < 0$ the λ–axis $\{\mu = 0, h = 0\}$ detaches from the swallow tail surface and forms a 1–dimensional thread. The inverse image of these points under the energy-momentum mapping is a pinched torus formed by the unstable equilibrium and its (coinciding) stable and unstable manifold. The thread does belong to the real part of the discriminant locus when interpreting (7.14) as a complex polynomial, but is not part of the (real)